Earth, Planets and Space
a SpringerOpen Journal

LETTER Open Access

Numerical modeling of trace element transportation in subduction zones: implications for geofluid processes

Akihiko Ikemoto[1*] and Hikaru Iwamori[1,2]

Abstract

This study presents the first numerical model for trace element transportation associated with dehydration and fluid migration from the subducting slab and aims to incorporate both fluid dynamical processes (e.g., flow mode and mass fluxes) in subduction zones and associated geochemical evidence (e.g., chemical compositions of arc lavas). The model includes temperature and flow structures associated with slab subduction and mantle-fluid two-phase flow, as well as phase relations of hydrous phases (e.g., dehydration-hydration reactions and melting) and trace element partitioning among the phases (solid, aqueous fluid, and melt). The model calculations show that if instantaneous chemical equilibrium is achieved associated with porous flow of slab-derived fluid, the elements expelled with the ascending fluid (e.g., Pb) are absorbed into the down-going hydrated mantle layer developed above the slab. As a result, these elements are considerably depleted in the resultant magma generated by fluid-flux melting in the core part of the mantle wedge, and it therefore fails to reproduce the geochemical characteristics of arc lavas. In contrast, if disequilibrium element transport (e.g., associated with channel flow) is assumed when the hydrated mantle layer liberates the fluid, then the key elements are delivered to the melting region to reproduce certain arc lava signatures. These results suggest that disequilibrium fluid transport in the wedge mantle, such as through channels, plays an important role in element cycling in subduction zones.

Keywords: Subduction; Slab-fluid; Arc magma; Numerical modeling; Trace element

Findings

Introduction

Subduction zones are one of the most tectonically active sites on Earth and are associated with remarkable amounts of material and energy transport. For example, it is believed that arc volcanism is derived from a combination of solid flow in the mantle wedge and fluid flow originating from the subducting slab. The slab-derived fluid (hereafter referred to as slab-fluid) migrates upwards in relation to buoyancy due to the density contrast and significantly reduces the melting temperature of the overlying mantle wedge by several hundred degrees with an input of some thousands parts per million H_2O (e.g., Green 1973; Iwamori 1998). Slab-fluid can also have chemical impact and is believed to metasomatize and enrich the wedge in incompatible elements. This process may explain the characteristic composition of arc magma, as well as the continental crust (e.g., relative Nb depletion and Pb positive spike in spidergram; Tatsumi and Eggins 1995). In addition, recent studies have indicated that slab dehydration and mantle metasomatism in subduction zones could lead to global mantle isotopic heterogeneity through fractionation between parent-daughter elements, e.g., Rb-Sr, Sm-Nd, and U-Th-Pb (Iwamori and Albarède 2008).

In order to quantify the potential importance of such element transport in subduction zones, the trace element and isotopic composition of subducted materials, slab-fluids, mantle wedge, and arc volcanic rocks have been extensively studied, involving elemental partitioning during dehydration and melting (e.g., Ishikawa and Nakamura 1992; Ayers 1998; Plank and Langmuir 1998; Pearce et al. 2005; Nakamura et al. 2008; Kimura et al. 2009). Such studies assume a simple configuration for

* Correspondence: ikemoto.a.aa@m.titech.ac.jp
[1]Department of Earth and Planetary Science, Tokyo Institute of Technology, 2-12-1 Oo-Okayama, Meguro, Tokyo 152-8550, Japan
Full list of author information is available at the end of the article

Springer

© 2014 Ikemoto and Iwamori; licensee Springer. This is an Open Access article distributed under the terms of the Creative Commons Attribution License (http://creativecommons.org/licenses/by/2.0), which permits unrestricted use, distribution, and reproduction in any medium, provided the original work is properly credited.

the fluid and element transport and use a box model for the subducted slab material, mantle wedge, and volcanic rocks, with prescribed elemental fluxes among the 'boxes.'

Fluid dynamical approaches can be complementary to the geochemical approaches mentioned above and have been constructed to quantitatively examine the fluid generation-migration and resultant melting in the mantle wedge (e.g., Iwamori 1998, 2007; Arcay et al. 2005; Cagnioncle et al. 2007; Hebert et al. 2009). Such numerical models provide constraints on the fluid fraction, migration velocity, and degree of melting that have been compared with the seismic velocity structures (Iwamori and Zhao 2000; Nakajima et al. 2005; Tonegawa et al. 2008). However, elemental transport has not been incorporated into those fluid dynamical models, and consequently, the actual mechanism for elemental transport has not been addressed.

In this study therefore, we combine geochemical and fluid dynamical approaches. The pioneering works of Spiegelman and McKenzie (1987) and McKenzie and O´Nions (1991) gave an analytical expression of the elemental fluxes associated with fluid flow interacting with the convecting solid in the mantle wedge, providing an idealized two-phase flow system that assumes a constant fluid fraction and partition coefficient. However, the study presented here includes a more realistic model setup, which allows a variable fluid fraction and partition coefficient based on a numerical two-phase flow model (Iwamori 1998) and recent knowledge of trace element partitioning between solid, melt, and aqueous fluid (e.g., Green et al. 2000; Kessel et al. 2005; Kimura et al. 2009). In addition, it is also the first numerical model to integrate a thermal flow structure, H_2O-bearing phase relations (including dehydration and melting reactions), and the transport of trace elements associated with fluid flow in subduction zones. Through this model, we aim to understand the elemental cycling and solid-fluid flow beneath arcs based on acquired geochemical data.

Model

In order to examine the chemical processes in subduction zones, we developed a numerical model for fluid processes based on Iwamori (1998). In this model, the phases present (aqueous fluid, melt, and solid) and the amount of H_2O in each phase are calculated based on parameterized phase relationships and H_2O solubility (Iwamori 1998, 2007).

The constant velocity and angle of a subducting slab are assumed to drive the circulation of solids in the mantle wedge by the process of dragging; for simplicity, mantle rheology is assumed to be isoviscous. Due to the density contrast and the solid flow, aqueous fluid is assumed to migrate as porous flow along the solid grain boundaries according to the pressure gradient, and if the water content is higher than the maximum water content, excess water is allocated to aqueous fluid. Melt is assumed to migrate with solid, and if the melt fraction exceeds 2 wt.%, the excess melt is assumed to be instantaneously extracted from the mantle (Iwamori and Zhao 2000; Nakajima et al. 2005; Zhu et al. 2013). In this model, the melt fraction depends on the water fraction, temperature, and pressure, but not on the degree of mantle depletion (i.e., major element composition) due to melt extraction, and this assumption is likely to result in an overestimate for the amount of produced melt; the validity of this will therefore be examined later. Water partitioning between solid and melt is assumed to reach equilibrium instantaneously, with a constant partition coefficient of 0.01 (Aubaud et al. 2008; Kohn and Grant 2006). The energy transported by the aqueous fluid and energy for phase transformation related to hydration and dehydration are neglected.

Based on these assumptions, the conservation of mass, momentum, and energy can be written as follows:

$$\frac{\partial\left(\rho_b C_b^{\mathrm{H_2O}}\right)}{\partial t} + \sum_i^{s,a,m} \nabla\cdot\left[\rho_i \phi_i C_i^{\mathrm{H_2O}} \boldsymbol{v}_i\right] = 0 \tag{1}$$

$$(v_x, v_z) = \left(\frac{\partial\Psi}{\partial z}, -\frac{\partial\Psi}{\partial x}\right) \tag{2}$$

$$\nabla^4\Psi = 0 \tag{3}$$

$$\boldsymbol{v}_a = \boldsymbol{v}_s - \frac{k_{\phi_a}}{\phi_a \eta_a}\,(1-\phi_a)\Delta\rho_a g \tag{4}$$

$$k_{\phi_a} = \left(R^2 {\phi_a}^n\right)/B \tag{5}$$

$$C_s^{\mathrm{H_2O}}/C_m^{\mathrm{H_2O}} = D_{s/m}^{\mathrm{H_2O}} \tag{6}$$

$$\left[\sum_{\mathrm{i}}^{\mathrm{s,m}}\left(\rho_i \phi_i {C_p}^i\right) + T\Delta S\frac{\partial\left(\rho_m \phi_m\right)}{\partial T}\right]\frac{\partial T}{\partial t} = K\nabla^2 T - \sum_i^{s,m}\left(\rho_i \phi_i {C_p}^i \boldsymbol{v}_i\cdot\nabla T - T\phi_i \alpha_i \boldsymbol{v}_i\cdot\nabla P\right) - T\Delta S\frac{\partial\left(\rho_m \phi_m\right)}{\partial\left(C_b^{\mathrm{H_2O}}\right)}\frac{\partial\left(C_b^{\mathrm{H_2O}}\right)}{\partial t} - T\Delta S\nabla\cdot\left(\rho_m \phi_m \boldsymbol{v}_m\right) \tag{7}$$

For phase i (m = melt, s = solid, a = aqueous fluid), ρ_i is density, ϕ_i is the volume fraction, $\boldsymbol{v}_i$ is the velocity vector, $C_i^{\mathrm{H_2O}}$ is the concentration of H_2O, and t is time. In Equation 1 for the local bulk system ($b = m + s + a$), ρ_b is the average density and $C_b^{\mathrm{H_2O}}$ is the average concentration of H_2O. Although the aqueous fluid dissolves a significant amount of silicate components in the pressure and temperature range of interest (Nakamura and Kushiro 1974; Fujii et al. 1997), $C_a^{\mathrm{H_2O}}$ (aqueous fluid) is assumed to

be unity. In Equations 2 and 3 for the solid flow, Ψ is the stream function. In Equation 4 for the flow of aqueous fluid (McKenzie 1984), k_{ϕ_a} is the permeability, η_a is the viscosity, $\Delta\rho_a$ is $\rho_s - \rho_a$, g is the acceleration due to gravity, R is the radius of the solid grain, and n and B are the constants ($n = 3$ and $B = 10^3$ are assumed after McKenzie (1984)). Although this formulation neglects viscous force in relation to compaction of the solid matrix and its associated nonlinear behavior (e.g., solitary porosity wave), it gives a reasonable estimate for the fluid velocity when the compaction length is small, which is considered likely to be the case with mantle melting (McKenzie 1984; Scott and Stevenson 1984). $D^{H_2O}_{s/m}$ is the partition coefficient of water between solid and melt. C^i_p is the heat capacity at constant pressure, α_i is the thermal expansion coefficient, ΔS is the entropy change associated with melting, and K is the thermal conductivity. For these constants, we set $\rho_s = \rho_m = \rho_b = 3.5 \times 10^3 \mathrm{kg\ m^{-3}}$, $\rho_a = 1.0 \times 10^3 \mathrm{kg\ m^{-3}}$, $\Delta\rho_a = 2.3 \times 10^3 \mathrm{kg\ m^{-3}}$, $\Delta\eta_a = 10^{-3} \mathrm{Pa\ s}$, $g = 9.8 \mathrm{m\ s^{-2}}$, $R = 1.0 \times 10^{-3} \mathrm{m}$, $\alpha_s = \alpha_m = 2.4 \times 10^{-5} \mathrm{K^{-1}}$, $\Delta S = 3.5 \times 10^2 \mathrm{J\ kg^{-1} K^{-1}}$, $K = 1.0 \times 10^{-6} \mathrm{m^2 s^{-1}}$, $C^s_p = C^m_p = 1.2 \times 10^3 \mathrm{J\ kg^{-1} K^{-1}}$ (Iwamori 1998).

In addition to phase relations and the transport of the solid-aqueous fluid melt system, the transport and partitioning of trace elements are formulated in this section in order to model trace element behavior in subduction zones. Trace elements are assumed to be partitioned instantaneously among the phases present (Ayers 1998; Kimura et al. 2009) and transported by the flow. Trace element transport and partitioning can therefore be written as follows:

$$\frac{\partial\left(\sum_i \rho_i \phi_i C^X_i\right)}{\partial t} + \sum_i \nabla \cdot \left[\rho_i \phi_i C^X_i \boldsymbol{v}_i\right] = 0 \tag{8}$$

$$C^X_s / C^X_m = D^X_{s/m} \tag{9}$$

$$C^X_s / C^X_a = D^X_{s/a} \tag{10}$$

where C^X_i is the composition of element X in phase i, $D^X_{s/m}$ is the partition coefficient between solid and melt, and $D^X_{s/a}$ is the partition coefficient between solid and aqueous fluid. Since elemental diffusion has a significantly smaller effect than the representative velocity of advective transport (e.g., Iwamori 1998), it has been neglected here. We calculate a bulk partition coefficient using an individual mineral-fluid and mineral-melt partition coefficients and the modal composition of minerals (Ayers and Watson 1993; Ayers et al. 1997; Kogiso et al. 1997; Green et al. 2000; Green and Adam 2003; Feineman et al. 2007; Usui et al. 2007; Kimura et al. 2009), together with their temperature dependence for garnet, clinopyroxene, orthopyroxene, chlorite, and amphibole (Garrido et al. 2005; Kessel et al. 2005; Moyen and Stevens 2006; Kimura et al. 2009, 2010). We then calculate the modal compositions of minerals for the mantle based on Kimura et al. (2009, 2010), as a function of pressure and temperature.

The numerical model has been developed for a two-dimensional vertical section of a subduction zone perpendicular to the trench axis. To compare the results with the observed compositions of arc basalts in the northeast Japan arc, we set a subducting velocity to 9 cm/year, and the angle to 30°, both assumed to be constant. This model includes oceanic lithosphere (with a thickness of 100 km), the overlying oceanic asthenosphere, oceanic crust (8 km), arc crust (30 km), and the mantle wedge between the subducting oceanic lithosphere and the arc crust (Figure 1). The analytic corner flow solutions are applied to express the solid flow in the mantle wedge and in the oceanic mantle (McKenzie 1969).

The thermal boundary conditions used in this study are as follows: At the vertical boundaries of the model box, the temperature depth profile is fixed in terms of time. In order to simulate subduction of the Pacific Plate beneath northeast (NE) Japan, a geotherm for the plate age of 130 million years (Myr) is applied to the oceanic side boundary, based on the one-dimensional cooling model of semi-infinite half-space (Turcotte and Shubert 1982) with an initial potential temperature of 1,350°C

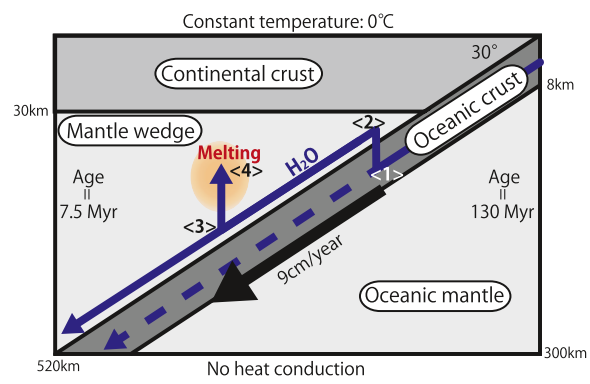

Figure 1 Geometrical configuration, boundary conditions, and H_2O transport of the model along the two-dimensional across-arc section. A constant subduction angle and the velocity of a straight slab are assumed. The boundary conditions for mass and energy transport are described in the main text. The thick (either solid or dashed) lines indicate the schematic transportation path of H_2O that are predicted in this numerical model, with specific transport reaction events labeled <1> to <4> as follows: At <1>, the subducting oceanic crust dehydrates, and a part of the H_2O within the oceanic crust is released upwards as aqueous fluid. At <2>, the ascending aqueous fluid hydrates the mantle wedge above the slab, and the hydrated mantle subducts along it. At <3>, the hydrated mantle dehydrates and forms an aqueous fluid column through which the fluid migrates upwards. At <4>, the ascending aqueous fluid lowers the solidus temperature to cause mantle melting.

(Parsons and Sclater 1977). Similarly, in order to reproduce the thermal condition beneath the Japan Sea, the geotherm for an oceanic plate of 7.5 Myr is used for the vertical boundary of the back-arc side, based on geothermometer with mantle-crust xenoliths Takahashi (1978). No heat conduction is assumed at the bottom boundary, whereas the surface is fixed at 0°C.

The boundary conditions concerning water are as follows: The top and left side of the box are permeable for fluid flow. For the subducting slab, the upper boundary allows permeable flow from the dehydrating slab and the water content on the oceanic side boundary is fixed, serving as a water source into the calculated system. The H_2O content of the subducting oceanic crust is assumed to be 3 wt.% (Rüpke et al. 2004) but is assumed to be zero under the oceanic crust, i.e., a dry peridotite for the subducting lithosphere (Iidaka and Suetsugu 1992; Kawakatsu and Yoshioka 2011).

We set a constant trace element composition on the oceanic side boundary (as with water), which consists of oceanic crust composed of altered oceanic crust (Kelley et al. 2003) and a depleted MORB mantle (DMM) (Workman and Hart 2005). The mantle composition flowing into the wedge is also assumed to have a DMM composition, while we neglect the composition of the arc crust because chemical reactions within the arc crust are not considered in this model. Other boundaries are permeable in terms of the elemental fluxes associated with both solid and fluid flows.

Results and discussion

Water transport and melting

Figure 2 shows the predicted distribution of (a) water content (in weight) in a local bulk system, (b) volume fraction of the aqueous fluid phase, and (c) the weight fraction of melt. The hydrated oceanic crust subducts and extensively dehydrates at a depth of 60 km, associated with the breakdown of amphibolite (at <1> in Figure 1). The generated aqueous fluid then migrates upwards to enter and hydrate the mantle wedge above the slab (Figure 1 <2>). This hydrated mantle then starts to dehydrate at 150 km depth (Figures 1 <3> and 2b), forming an aqueous fluid column through which the fluid migrates upwards to reach a high-temperature area at the central part of the mantle wedge (Figure 1 <4>), and causes mantle melting by invoking a lowering of the solidus temperature. These results are essentially the same as those in Iwamori (1998), but our study includes a hydrated layer (several thousand parts per million H_2O) measuring 30-km thick, which developed just above the slab at a depth greater than 150 km (Figure 2b), and is hereafter referred to as the 'material boundary layer.' It consists of nominally anhydrous minerals and is considered to play an important role in deep water subduction (Iwamori 2007; Iwamori and Nakakuki 2013) and element transport, which will be discussed later. It is noted for clarity that the material boundary layer is saturated with aqueous fluid at a depth range between 150 and 200 km, where both the hydrated material boundary layer (Figure 2a) and the aqueous fluid phase (Figure 2b) coexist.

When the melt is generated, H_2O is preferentially partitioned into it, up to 25 wt.% under PT conditions in the mantle wedge (Iwamori 1998). If melt extraction occurs, the H_2O contained in the melt is also extracted from a rock packet, which increases the solidus temperature and suppresses subsequent melting of the rock packet. This suppression is seen in Figure 2d (the melting region (A) in Figure 2d), where melt is extracted along the nearly horizontal streamline (from left to right along the dotted lines in Figure 2d) consisting of an initially dry solid. No subsequent melting occurs along the streamline towards the wedge corner. Exceptionally, the rock packet melts when it is significantly hydrated within an aqueous fluid column with an H_2O content of 0.2 wt.% (melting region (B) in Figure 2d). As will be shown later, the melt compositions in (A) and (B) of Figure 2d are distinct, reflecting the difference in the melting conditions: (A) exhibits a higher temperature, lower water content, and lower melting degree; and (B) has a lower temperature, higher water content, and higher melting degree. It is noted that the melting degree, which is not shown, differs from the information presented in Figure 2d, which shows melt fraction present in each rock packet. Considering the geometry of the streamlines (dotted lines in Figure 2d), (B) in Figure 2d corresponds to the remelting of the residue from the melting in (A) of Figure 2d, which results in the higher melting degree in (B).

In the additional file, we present an additional calculation in which we incorporate the effects of mantle depletion in the major elements, by integrating the melt extraction and by calculating the subsequent melting according to the degree of depletion. Additional file 1: Figure S1 shows that the overall melting structure remains essentially the same, even when the effects of mantle depletion in major elements are taken into account (*cf.* Figure 2c). The following discussions will therefore be based on the model results, without incorporating the 'major element depletion effects' as in Figure 2.

Trace element composition of magma

Figure 3 shows DMM-normalized spidergrams of the melt trace element compositions, together with average lava compositions of the NE Japan arc (Kimura and Yoshida 2006; Kimura and Stern 2009). The melt compositions exhibit two different patterns. One is a relatively smooth pattern of generally high elemental abundances

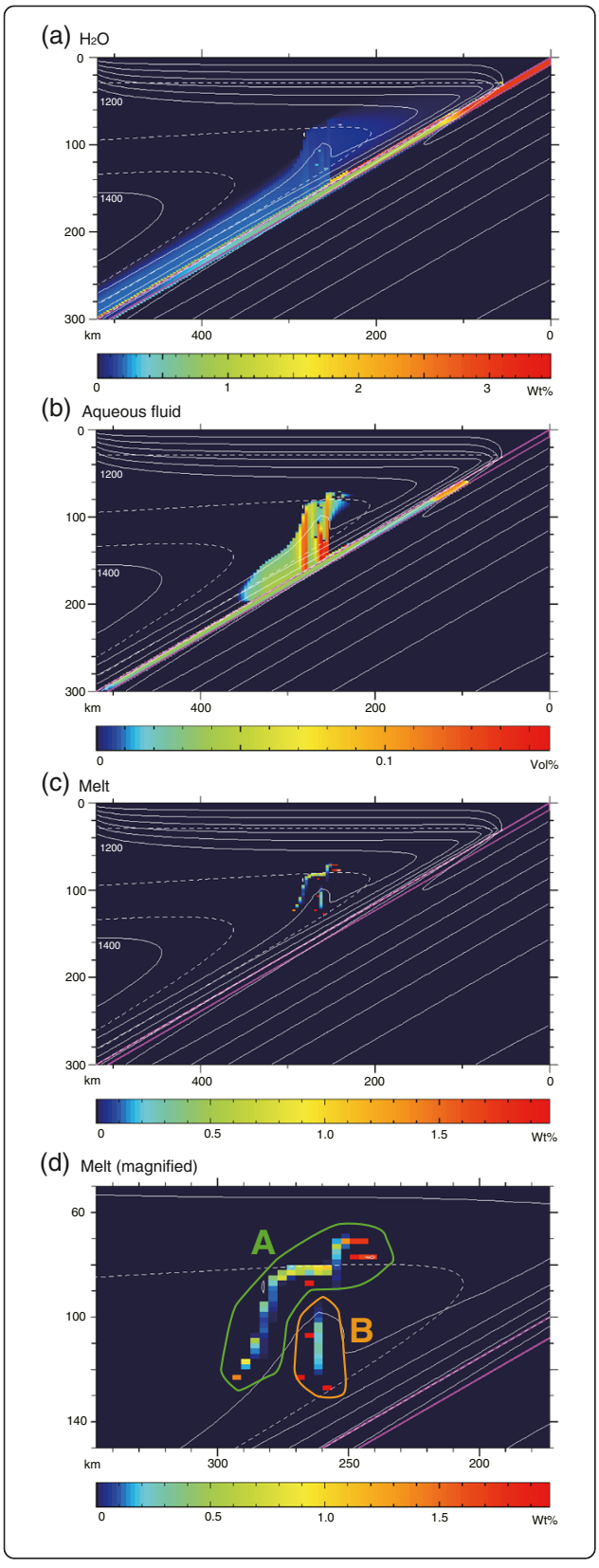

Figure 2 Water and melt distributions predicted in the model calculation. The upper right corner corresponds to the trench. The white solid lines indicate temperature contours with 200°C intervals (for 200°C, 400°C, 600°C, 800°C, 1,000°C, 1,200°C, and 1,400°C), and the white dotted lines indicate the streamline. The purple solid lines indicate the lower and upper boundaries of the subducting oceanic crust. **(a)** Water (in weight) in a local bulk system. **(b)** Aqueous fluid fraction (in volume). **(c)** Melt fraction (in weight). **(d)** A magnified view of the central part of **(c)**. In **(d)**, orange and green circles correspond to two different melting regimes, as explained in the main text.

(green lines in Figure 3) that reflects a relatively small degree of DMM melting without much affect from the elements derived by fluid in the region (A) of Figure 2b. This smooth pattern can be approximated by a melt composition that corresponds to hypothetical pure DMM melting (purple line in Figure 3), confirming an insignificant compositional modification of the source DMM mantle by the aqueous fluid.

The other pattern is not smooth and consists of generally low abundances (orange lines in Figure 3), in particular the relative depletion of Nb and Ta and the relative enrichment of Rb, which reflects the higher degree of melting of a source that has been affected by both prior melt extraction and concurrent fluid addition in region (B) (Figure 2b). These melt compositions, as well as the direct inspection of fluid compositions in the numerical results, show that the aqueous fluids added to regions (A) and (B) are very diluted in terms of trace element abundances (except for the relative enrichment of Rb that affects the source region (B) where the overall trace element abundances in the solid have already been lowered by prior melt extraction). The reason for the extreme dilution of the aqueous fluids generated at point <3> of Figure 1 is investigated in detail below.

There are certain compositional similarities and differences between the lavas from NE Japan arc and those of the model melt (Figure 3). The overall elemental abundances of the lavas and the model melt overlap in relation to Rb, Nb, Ta, and the light to mid-rare earth elements (mid-REEs) (i.e., La to Dy). However, the lava compositions show higher ranges for Ba, Th, U, Pb, Sr, and heavy REEs (Figure 3). Of these, Pb is one of the key elements that characterize arc lavas with relative enrichment (e.g., Tatsumi and Eggins 1995) and is investigated here in detail. Figure 4 shows the Pb abundances in solid and aqueous fluid, and this clearly indicates that Pb is liberated from the oceanic crust and incorporated into the mantle just above the slab, forming a hydrated Pb-rich layer. Then this hydrated mantle layer subducts to increase pressure and again liberates the aqueous fluid that contains Pb (which is associated with the breakdown of serpentine and chlorite). Lead is then partitioned into

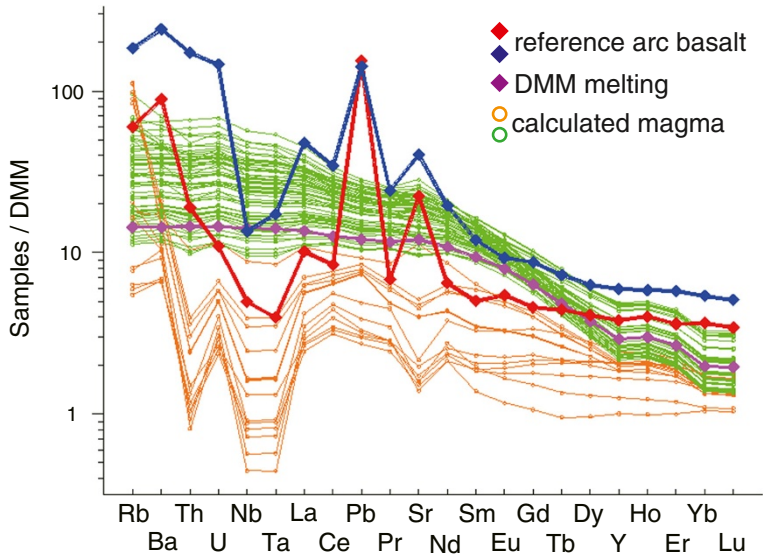

Figure 3 Spidergram for the calculated melt. The melt composition is normalized by the DMM composition, which is assumed as an initial mantle composition (before fluid flux is introduced) in our model. The green and orange lines correspond to the melt compositions produced in regions (A) and (B) of Figure 2d, respectively. Each line represents a local instantaneous melt composition. The red line represents the frontal arc basalt from NE Japan, and the blue line for the rear arc basalts (Kimura and Yoshida 2006; Kimura and Stern 2009). For comparison, an average melt composition corresponding to hypothetical pure DMM melting is shown as the purple line, with the same melting degrees and partition coefficients as in the model result.

the solid mantle as it ascends upwards with the fluid (Figure 4). As a result, virtually, all of the Pb is absorbed into the solid before it reaches the melting region (hence, no positive Pb spike is seen in Figure 3) and is dragged down to the deep mantle with the descending material boundary layer (Figure 4a). In this calculation result, the Pb concentration in the hydrated material boundary layer is 0.3 ppm, in which the most Pb-enriched phase is garnet (1.1 ppm Pb). These concentration levels are within the experimental range (see Kessel et al. 2005 and the references of Kimura et al. 2009, in which the relevant partition coefficients are derived for the model calculation) and are judged to be below the saturation level for a solid. An additional calculation in the Additional file 1: Figure S2 incorporates subducted sediments into the model that contains more Pb than the altered oceanic crust and again shows that virtually all the Pb expelled from the slab is absorbed into the solid material boundary layer before it reaches the melting region. Similarly, fluid mobile elements (e.g., Rb, Th, Sr) are expelled from the slab and are absorbed into the material boundary layer to be dragged down to the deep mantle.

The thickness of the material boundary layer that absorbs a specific element depends on the concentration and the partition coefficient of the specific element. For example, Rb requires a thicker layer of 30 km in order to be absorbed, compared with that of Sr which requires a layer of 15 km in thickness. These material boundary layers absorb the fluid-mobile elements, resulting in no relative enrichment of elements, which characterizes the arc magmas, for the model melt (Figure 3). This leads us to consider that if fluid migration occurs in a chemical disequilibrium with the surrounding solid mantle, these elements could reach a melting region that fertilizes the resultant melt. Iwamori and Nakakuki (2013) demonstrate that the seismic velocity structures beneath the NE Japan arc, in terms of variability within the ΔVp-ΔVs relationship, correspond to the existence of a fracture system in the mantle wedge, and it is known that fluids in such a fracture system have a reduced contact area with the surrounding mantle, possibly resulting in chemical disequilibrium due to slow elemental diffusion in the solid (Iwamori 1993).

In order to simulate such a possible disequilibrium situation, firstly, once the fluid is expelled from the hydrated mantle just above the slab, we ignore the elemental partitioning between the fluids and the solids in the mantle wedge. The element abundances in the fluid phase are then preserved until the fluid reaches the melting region. The resultant melt compositions are shown in Figure 5, where the Ba, Pb, and Sr abundances in the model melt are elevated and are seen to overlap the observed ranges. However, in relation to Th and U, which are thought to be fluid mobile elements, the abundance elevation is not large enough to account for those in the observations. These elements are not liberated from the hydrated layer just above the slab at point <3> in Figure 1 due to their preferential partitioning into

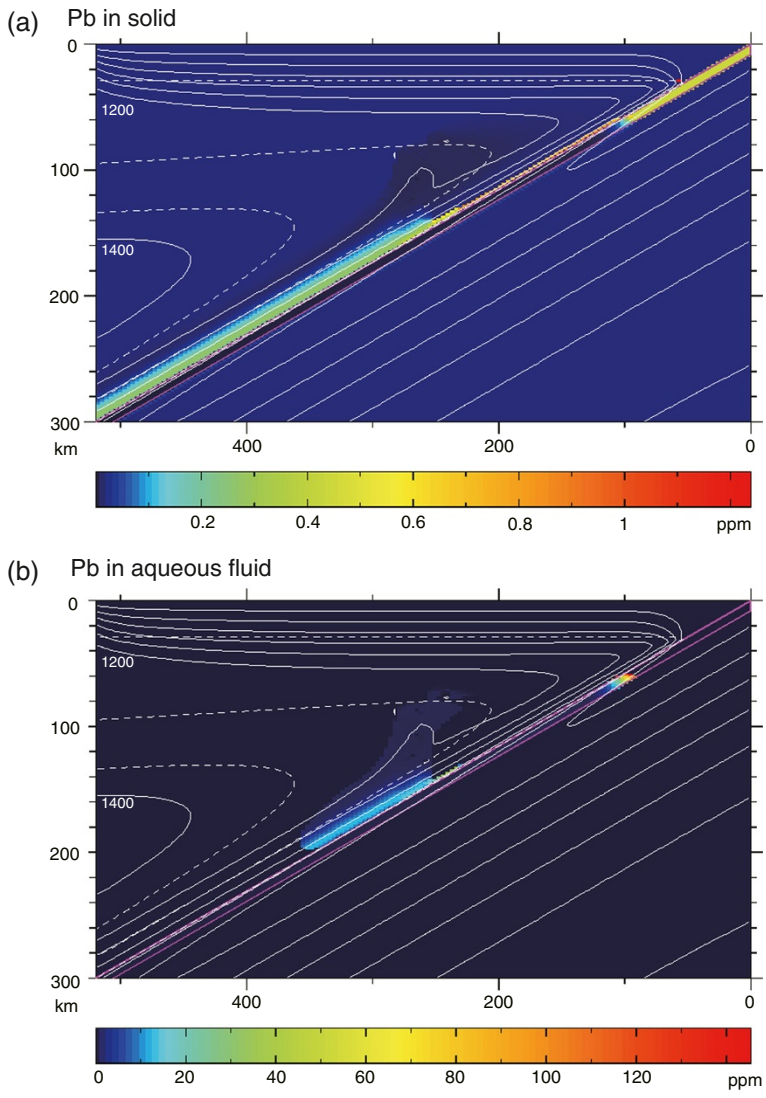

Figure 4 Calculated distribution of Pb. (a) Pb concentration in solid. **(b)** Pb concentration in aqueous fluid. The Pb concentration in aqueous fluid is color-coded only where the fluid phase is present in respective grid cells and is shown everywhere else with a 'background zero ppm' concentration (i.e., the dark blue region). The white solid and dotted lines correspond to the temperature contours (with 200°C intervals) and the streamline, respectively, as in Figure 2. The purple solid lines indicate the lower and upper boundaries of the subducting oceanic crust (as in Figure 2), and the boundary conditions of mass and energy conservation are the same as in Figure 2.

the garnet in solid at relatively low temperatures (Kessel et al. 2005; Kimura et al. 2009). Figure 6 shows color contour maps for the partition coefficients of U, Th, Pb, and Yb, indicating that those of U and Th are relatively temperature sensitive along the possible slab geotherms, especially around the dehydration point <3> of Figure 1 (two solid lines and the square points in Figure 6, respectively). In the current model, a constant viscosity for the mantle flow is assumed for simplicity, and this tends to suppress temperature along the subducting slab (e.g., van Keken et al. 2002) and elemental partitioning to the fluid at the dehydration condition (e.g., Kessel et al. 2005), when compared to the alternative thermal model (Syracuse et al. 2010; Figure 6).

Although the model melts also show an abundance of heavy REEs (i.e., Y to Lu in Figure 5), these are lower than those of the observed range. The low abundances reflect the dominant involvement of garnet upon melting, because heavy REEs are preferentially absorbed into garnet (Green et al. 2000). In this model, the instantaneous melt extraction has been assumed (i.e., the chemical reactions between the melt and the solid during melt ascent have been ignored). If the melt that originated in the garnet stability field ascends with a continuous re-

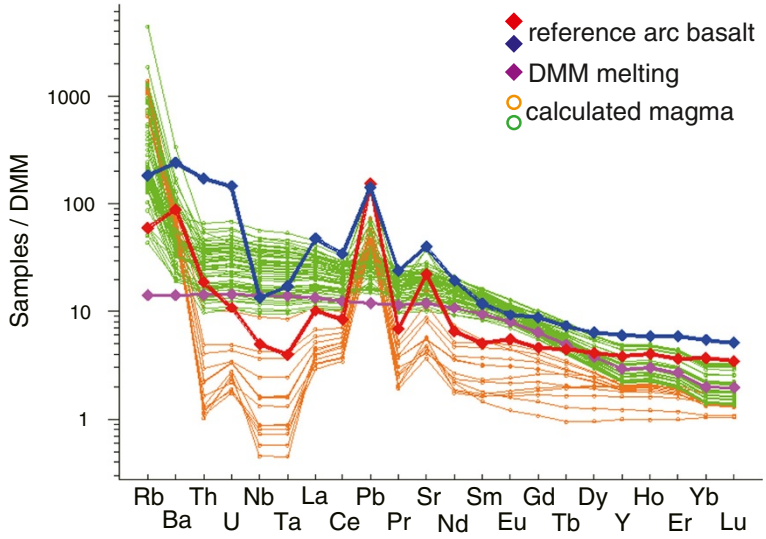

Figure 5 Spidergram for melt calculated by the disequilibrium model. The DMM-normalized melt composition is shown and is predicted by the model assuming disequilibrium fluid transport (see main text for details). The criteria for different color lines are the same as in Figure 3.

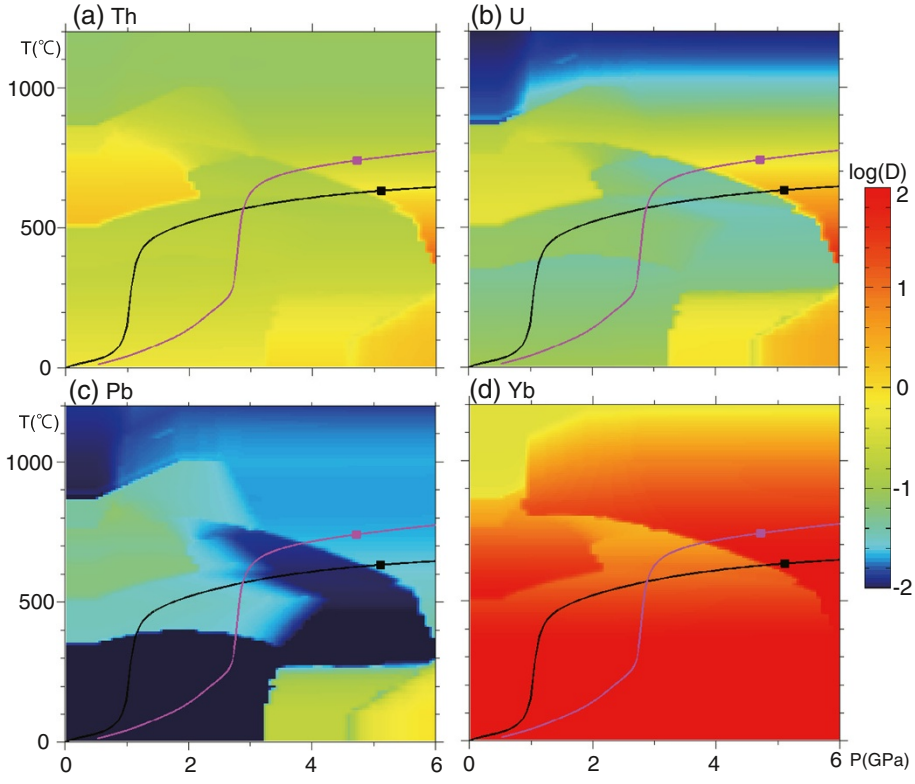

Figure 6 Partition coefficient (*D*) distribution in pressure-temperature (PT) space. Logarithm of the partition coefficients (log*D*) between mantle and aqueous fluid within the investigated PT space. **(a)** Th, **(b)** U, **(c)** Pb, and **(d)** Yb. The temperature and pressure ranges and the color contour scale are the same for **(a)** to **(d)**. The solid lines indicate along-slab (slab-mantle wedge interface) geotherms for two different thermal models. The squares indicate PT conditions at the point at which the hydrated mantle dehydrates (corresponding to <3> in Figure 1). The black line and square are from our model calculation, and the purple line and square are based on Syracuse et al. (2010).

equilibration with the spinel peridotite at shallower depths, it is likely that the heavy REE depletion may be relaxed to some extent.

These similarities and differences in chemical compositions between the model melt and the actual lavas provide new insights as follows: The element transport in subduction zones sensitively reflects the PT condition (which controls the partition coefficients) and in order to explain the observed positive spikes of several key elements including Pb, the fluid liberated from the slab must deliver those elements to the melting regions without being significantly absorbed in the down-going mantle materials. We therefore suggest that a disequilibrium fluid transport system through channels exists, such as a fracture system in the wedge mantle. By improving the model assumption and our knowledge on the partition coefficients between fluid, melt, and solid phases, we strive to better understand the elemental cycling in subduction zones.

Additional file

Additional file 1: Supplementary numerical results for two potentially important factors that have been neglected in the discussion presented in the main text. Figure S1. Calculated distribution of melt, taking into account the major element depletion effects on melting. **Figure S2.** Calculated distribution of Pb in solid, taking account of subducting sediments.

Competing interests
The authors declare that they have no competing interests.

Authors' contributions
AI designed the numerical model, constructed the simulation code, carried out the calculation, and wrote the manuscript. HI designed the numerical model, checked the code, and wrote the manuscript. Both authors read and approved the final manuscript.

Acknowledgements
We are very grateful to Hitomi Nakamura, Jun-Ichi Kimura, Shyunsuke Horiuchi, and Morihisa Hamada for their considerable help in constructing the numerical model. We also thank Kenta Ueki and Masaoki Uno for their critical discussion.

Author details
[1]Department of Earth and Planetary Science, Tokyo Institute of Technology, 2-12-1 Oo-Okayama, Meguro, Tokyo 152-8550, Japan. [2]Japan Agency for Marine-Earth Science and Technology, 2-15 Natsushima-cho, Yokosuka-shi, Kanagawa 237-0061, Japan.

Received: 29 November 2013 Accepted: 24 March 2014
Published: 30 April 2014

References
Arcay D, Tric E, Doin MP (2005) Numerical simulations of subduction zones: effect of slab dehydration on the mantle wedge dynamics. Phys Earth Planet Inter 149:133–153, doi:10.1016/j.pepi.2004.08.020

Aubaud C, Hirschmann MM, Withers AC, Hervig RL (2008) Hydrogen partitioning between melt, clinopyroxene, and garnet at 3 GPa in a hydrous MORB with 6 wt.% H_2O. Contrib Mineral Petrol 156:607–625

Ayers J (1998) Trace element modeling of aqueous fluid–peridotite interaction in the mantle wedge of subduction zones. Contrib Mineral Petrol 132:390–404, doi:10.1007/s004100050431

Ayers JC, Watson EB (1993) Rutile solubility and mobility in supercritical aqueous fluids. Contrib Mineral Petrol 114:321–330, doi:10.1007/BF01046535

Ayers JC, Dittmer SK, Layne GD (1997) Partitioning of elements between peridotite and H_2O at 2.0-3.0 GPa and 900-1100°C, and application to models of subduction zone processes. Earth Planet Sci Lett 150:381–398, doi:10.1016/S0012-821X(97)00096-4

Cagnioncle AM, Parmentier EM, Elkins-Tanton LT (2007) Effect of solid flow above a subducting slab on water distribution and melting at convergent plate boundaries. J Geophys Res 27:425–428, doi:10.1029/2007JB004934

Feineman MD, Ryerson FJ, DePaolo DJ, Plank T (2007) Zoisite-aqueous fluid trace element partitioning with implications for subduction zone fluid composition. Chem Geol 239:250–265, doi:10.1016/j.chemgeo.2007.01.008

Fujii T, Mibe K, Yasuda A (1997) "Magma ocean did not exist?" (in Japanese). Kagaku 67:179–183

Garrido CJ, Sánchez-Vizcaíno VL, Gómez-Pugnaire MT, Trommsdorff V, Alard O, Godard M (2005) Enrichment of HFSE in chlorite–harzburgite produced by high-pressure dehydration of antigorite–serpentinite: implications for subduction magmatism. Geochem Geophys Geosyst, doi:10.1029/ 2004GC000791

Green DH (1973) Experimental melting studies on a model upper mantle composition at high pressure under water-saturated and water-undersaturated conditions. Earth Planet Sci Lett 19:37–53, doi:10.1016/0012-821X(73)90176-3

Green TH, Adam J (2003) Experimentally-determined trace element characteristics of aqueous fluid from partially dehydrated mafic oceanic crust at 3.0 GPa, 650-700°C. Eur J Mineral 15:815–830, doi:10.1127/0935-1221/2003/0015-0815

Green TH, Blundy JD, Adam J, Yaxley GM (2000) SIMS determination of trace element partition coefficients between garnet, clinopyroxene and hydrous basaltic liquids at 2–7.5 GPa and 1080–1200°C. Lithos 53:165–187, doi:10.1016/S0024-4937(00)00023-2

Hebert LB, Antoshechkina P, Asimow P, Gurnis M (2009) Emergence of a low-viscosity channel in subduction zones through the coupling of mantle flow and thermodynamics. Earth Planet Sci Lett 278:243–256, doi:10.1016/j.epsl.2008.12.013

Iidaka T, Suetsugu D (1992) Seismological evidence for metastable olivine inside a subducting slab. Nature 356:593–595, doi:10.1038/356593a0

Ishikawa T, Nakamura E (1992) Boron isotope geochemistry of the oceanic crust from DSDP/ODP Hole 504B. Geochim Cosmochim Acta 56:1633–1639

Iwamori H (1993) A model for disequilibrium mantle melting incorporating melt transport by porous and channel flows. Nature 366:734–737, doi:10.1038/366734a0

Iwamori H (1998) Transportation of H_2O and melting in subduction zones. Earth Planet Sci Lett 160:65–80, doi:10.1016/S0012-821X(98)00080-6

Iwamori H (2007) Transportation of H_2O beneath the Japan arcs and its implications for global water circulation. Chem Geol 239:182–198, doi:10.1016/j.chemgeo.2006.08.011

Iwamori H, Albarède F (2008) Decoupled isotopic record of ridge and subduction zone processes in oceanic basalts by independent component analysis. Geochem Geophys Geosyst, doi:10. 2007GC001753

Iwamori H, Nakakuki T (2013) Fluid processes in subduction zones and water transport to the deep mantle. In: Karato S (ed) Physics and chemistry of the deep earth. Elsevier, Amsterdam

Iwamori H, Zhao D (2000) Melting and seismic structure beneath the northeast Japan arc. Geophys Res Lett 27:425–428, doi:10.1029/1999GL010917

Kawakatsu H, Yoshioka S (2011) Metastable olivine wedge and deep dry cold slab beneath southwest Japan. Earth Planet Sci Lett 303:1–10, doi:10.1016/j.epsl.2011.01.008

Kelley KA, Plank T, Ludden J, Staudigel H (2003) Composition of altered oceanic crust at ODP Sites 801 and 1149. Geochem Geophys Geosyst, doi:10.1029/2002GC000435

Kessel R, Schmidt MW, Ulmer P, Pettke T (2005) Trace element signature of subduction-zone fluids, melts and supercritical liquids at 120–180 km depth. Nature 437:724–727, doi:10.1038/nature03971

Kimura JI, Stern RJ (2009) Neogene volcanism of the Japan island arc: the K-h relationship revisited. In: Spencer JE, Titley SR (eds) Ores and orogenesis: circum-Pacific tectonics, geologic evolution, and ore deposits. Arizona Geological Society, Tucson

Kimura JI, Yoshida T (2006) Contributions of slab fluid, mantle wedge and crust to the origin of Quaternary lavas in the NE Japan arc. J Petrol 47:2185–2232, doi:10.1093/petrology/egl041

Kimura JI, Hacker BR, van Keken PE, Kawabata H, Yoshida T, Stern RJ (2009) Arc Basalt Simulator version 2, a simulation for slab dehydration and fluid-fluxed

mantle melting for arc basalts: modeling scheme and application. Geochem Geophys Geosyst, doi:10.1029/2008GC002217
Kimura JI, Kent AJR, Rowe MC, Katakuse M, Nakano F, Hacker BR, van Keken PE, Kawabata H, Stern RJ (2010) Origin of cross-chain geochemical variation in Quaternary lavas from the northern Izu arc: using a quantitative mass balance approach to identify mantle sources and mantle wedge processes. Geochem Geophys Geosyst, doi:10.1029/2010GC003050
Kogiso T, Tatsumi Y, Nakano S (1997) Trace element transport during dehydration processes in the subducted oceanic crust: 1. Experiments and implications for the origin of ocean island basalts. Earth Planet Sci Lett 148:193–205, doi:10.1016/S0012-821X(97)00018-6
Kohn SC, Grant KJ (2006) The partitioning of water between nominally anhydrous minerals and silicate melts. Rev Mineral Geochim 62:231–241, doi:10.2138/rmg.2006.62.10
McKenzie DP (1969) Speculations on the consequence and causes of plate motions. Geophys J R Astron Soc 18:1–32, doi:10.1111/j.1365-246X.1969.tb00259.x
McKenzie D (1984) The generation and compaction of partially molten rock. J Petrol 25:713–765
McKenzie D, O´Nions RK (1991) Partial melt distributions from inversion of rare earth element concentrations. J Petrol 32:1021–1091
Moyen JF, Stevens G (2006) Experimental constraints on TTG petrogenesis: implications for Archean geodynamics. In: Been K, Mareschal JC, Condie KC (eds) Archean geodynamics and environments, vol 164. American Geophysical Union, Washington, pp 149–175
Nakajima J, Takei Y, Hasegawa A (2005) Quantitative analysis of the inclined low-velocity zone in the mantle wedge of northeastern Japan: a systematic change of melt-filled pore shapes with depth and its implications for melt migration. Earth Planet Sci Lett 234:59–70, doi:10.1016/j.epsl.2005.02.033
Nakamura Y, Kushiro I (1974) Composition of the gas phase in Mg_2SiO_4–SiO_2–H_2O at high pressures. Carnegie Inst Washington Yearb 73:266–268
Nakamura H, Iwamori H, Kimura JI (2008) Geochemical evidence for enhanced fluid flux due to overlapping subducting plates. Nat Geosci 1:380–384, doi:10.1038/ngeo290
Parsons B, Sclater JG (1977) An analysis of the variation of ocean floor bathymetry and heat-flow with age. J Geophys Res 82:803–827, doi:10.1029/JB082i005p00803
Pearce JA, Stern RJ, Bloomer SH, Fryer P (2005) Geochemical mapping of the Mariana arc-basin system: implications for the nature and distribution of subduction components. Geochem Geophys Geosyst, doi:10.1029/2004GC000895
Plank T, Langmuir CH (1998) The chemical composition of subducting sediment and its consequences for the crust and mantle. Chem Geol 145:325–394, doi:10.1016/S0009-2541(97)00150-2
Rüpke LH, Morgan JP, Hort M, Connolly JAD (2004) Serpentine and the subduction zone water cycle. Earth Planet Sci Lett 223:17–34, doi:110.1016/j.epsl.2004.04.018
Scott DR, Stevenson DJ (1984) Magma solitons. Geophys Res Lett 11:1161–1164, doi:10.1029/GL011i011p01161
Spiegelman M, McKenzie D (1987) Simple 2-D models for melt extraction at mid-ocean ridges and island arcs. Earth Planet Sci Lett 83:137–152, doi:10.1016/0012-821X(87)90057-4
Syracuse EM, van Keken PE, Abers GA (2010) The global range of subduction zone thermal models. Phys Earth Planet Inter 183:73–90, doi:10.1016/j.pepi.2010.02.004
Takahashi E (1978) Petrologic model of the crust and upper mantle of the Japanese island arcs. Bull Volcanol 41:529–547
Tatsumi Y, Eggins S (1995) Subduction-zone magmatism. Blackwell, Cambridge
Tonegawa T, Hirahara K, Shibutani T, Iwamori H, Kanamori H, Shiomi K (2008) Water flow to the mantle transition zone inferred from a receiver function image of the Pacific slab. Earth Planet Sci Lett 274:346–354, doi:10.1016/j.epsl.2008.07.046
Turcotte DL, Shubert G (1982) Geodynamics: applications of continuum physics to geological problems. Wiley, New York
Usui T, Kobayashi K, Nakamura E, Helmstaedt H (2007) Trace element fractionation in deep subduction zones inferred from a lawsonite-eclogite xenolith from the Colorado Plateau. Chem Geol 239:336–351, doi:10.1016/j.chemgeo.2006.08.009
van Keken PE, Kiefer B, Peacock SM (2002) High-resolution models of subduction zones: implications for mineral dehydration reactions and the transport of water into the deep mantle. Geochem Geophys Geosyst, doi:10.1029/2001GC000256
Workman RK, Hart SR (2005) Major and trace element composition of the depleted MORB mantle (DMM). Earth Planet Sci Lett 231:53–72, doi:10.1016/j.epsl.2004.12.005
Zhu GZ, Gerya TV, Tackley PJ, Kissling E (2013) Four-dimensional numerical modeling of crustal growth at active continental margins. J Geophys Res 118:4682–4698, doi:10.1002/jgrb.50357

doi:10.1186/1880-5981-66-26
Cite this article as: Ikemoto and Iwamori: **Numerical modeling of trace element transportation in subduction zones: implications for geofluid processes.** *Earth, Planets and Space* 2014 **66**:26.

Submit your manuscript to a SpringerOpen journal and benefit from:

- ► Convenient online submission
- ► Rigorous peer review
- ► Immediate publication on acceptance
- ► Open access: articles freely available online
- ► High visibility within the field
- ► Retaining the copyright to your article

Submit your next manuscript at ► springeropen.com